Power Flow-Based Adaptive Generator Controls

Manuel Garcia, Scott Backhaus, and Russell Bent

***Abstract*—Electrical transmission grids rely on generator inertia, frequency droop control, and automatic voltage regulation (AVR) to maintain transient stability following power system contingencies such as faults. Generator inertia and frequency droop modify real power and primarily act in a "global" sense, i.e. they respond to the global transient imbalance of generation and load. Under high loading or extended fault durations, this global response may be insufficient to maintain transient stability. We propose additional automatic controls that create a local real power response to a contingency. Specifically, for every generator, we add an input to its turbine governor proportional to the deviation of the power flows on the generator's adjacent transmission lines from a nominal steady state. Using dynamical simulation of the post-contingency dynamics, we optimize over the *gains* of these power flow feedbacks to improve the transient stability of the network. The optimization step enables these controls to be adaptive to changing power system conditions. We demonstrate the effectiveness of this approach by incrementally loading a test network while optimizing the power flow feedback gains to delay the onset of transient instability for a given critical clearing time applied to all contingencies.**

Keywords*—*Contingency planning, frequency stability, voltage stability, remedial action schemes, adaptive control, simulation-based.

I. Introduction

Contingencies such as faults, line trips, and dropped generation/load excite dynamical responses in power systems. These power systems rely on physics (generator inertia) and two basic controls (speed droop and automatic voltage regulation) to maintain stable transient dynamics [5]. A normally-cleared fault provides an example of how these different effects combine to promote stability. During the period while a fault is applied (i.e. the "fault-on" period), the suppression of generator terminal voltage reduces the ability of a generator to deliver real power to the transmission network, however, the generator's mechanical input power remains nearly constant over the short fault-on period. The power imbalance causes the generator to accelerate to higher rotational speeds and advance in phase relative to the rest of the power system. For a generator with larger inertia, the acceleration and phase advance are smaller, and the chance of the generator losing synchrony with the rest of the power system is reduced.

At slower time scales, the increase in the rotational speed causes the speed droop control to lower the mechanical power input to the generator to counteract the acceleration [5]. Inertia and speed droop are the two direct controls on generator speed. Automatic voltage regulation (AVR) provides an indirect effect on generator real power output by regulating a generator's terminal voltage to a reference voltage. In some circumstances, a power system stabilizer (PSS) may also be employed to modify a generator's terminal voltage to further regulate its real power output, however, the effect of the PSS is generally focused on small signal stability, i.e. increasing the damping of inter-area oscillations [5], and not on transient stability.

When a power system is stressed, the combination of inertia, speed droop and AVR may not be sufficient to maintain transient stability for all disturbances. In these circumstances, the power system becomes congested—the dispatch of generation becomes constrained limiting access to inexpensive generation and increasing the overall cost of electricity by forcing the dispatch of more expensive resources. In these circumstances, additional controls may be effective in restoring stability and access to the least expensive generation. However, for high reliability, any additional control acting on transient dynamics should retain one very reliable aspect of speed droop and AVR; the control should be distributed requiring only local measurements without reliance on significant communications.

In this manuscript, we propose and investigate the use of power flows on lines adjacent to a generator as an additional input to the generator's controls. Specifically, this new control measures the deviation of power flows on transmission lines adjacent to a generator from a nominal steady state, multiplies these deviations by individual gains, and adds the results to the frequency deviation term at the input to the generator's governor. We retain both speed droop and AVR and integrate the new additional control with these existing controls. A similar control structure was first proposed in [4], but was only explored in the context of automatic generation control (AGC), i.e. at time scales slower than transient dynamics where the control objective is focused on restoration of the nominal system frequency. Here, we extend the investigation of this new control to transient stability.

The proposed control has several potentially advantageous properties. First, the structure of the proposed control ensures that local generators respond to the disturbance, e.g. for a normally-cleared fault, the deviation of power line flows is contained to the region around the fault, and the structure of the control creates a local response to this disturbance. Second, a fault at a specific bus will create a characteristic pattern of line flows. By allowing independent gains for power flow deviations on different lines, the response of a generator can be tailored to different faults. Finally, the gains are determined by an optimization procedure that also allows the generator response to be adaptive—a property that will become increasingly important as more intermittent generation is introduced into power systems and power flows become more variable. Specifically, a set of gains determined for one pattern of power flows may actually degrade transient stability for a different pattern of power flows that could be reached by normal variability of intermittent generation. The proposed optimization procedure allows for adaptation to these variations.

Our adaptive optimization procedure is described in detail later in the manuscript. Here, we provide a brief overview. Consider a set of credible contingencies $\mathcal{C}$ that potentially impact secure power system operations. In this work, the set $\mathcal{C}$ consists of cleared faults C_i, each with a maximum clearing time $t_{0,i}$. A stability screening tool is used to partition $\mathcal{C}$ into a subset $\mathcal{S}$ that exhibits stable dynamics and a subset $\mathcal{U}$ exhibits dynamics approaching instability. In this work, the segregation into $\mathcal{S}$ and $\mathcal{U}$ is done using time simulation [6] and a penalty function that approximates the proximity to dynamical instability. However, any stability screening method that provides a continuous measure of instability can be used. Next, we use interior point [8] to find a set of power flow deviation gains that lower the penalty function value for the subset $\mathcal{U}$ ultimately moving them into subset $\mathcal{S}$.

The controls proposed in this manuscript are related to other fast acting wide-area and local-area controls that have received recent attention. Work on wide-area control [2] has focused on the design of sparse control structures that utilize system-wide measurements, e.g. from phasor measurement units (PMU). In this case, the desired control structure is sparse to minimize the amount of communication required to distribute the PMU measurements to the control points. Closer to the work considered here, others have considered distributed controllers to increase system damping designed using centralized computation [3] or neural networks [1]. However, these studies only utilize local frequency measurements and do not consider the power flow terms considered in this manuscript. Adaptive control techniques have also been used to implement Remedial Action Schemes (RAS). [9] presents an Adaptive RAS that updates circuit breaker control plans under specific severe contingencies using Lyapunov methods. Our adaptive generator controls potentially reduces the number of contingencies for which RAS's are necessary (i.e. our control reduces the number of severe contingencies necessary for the Adaptive RAS to consider in [9]).

The rest of this manuscript is organized as follows. Section II describes the test case, dynamic model, simulation methods and our innovative distributed control structure. Section III presents our stability screening tool, defines our stability metric and describes the adaptive portion of our control structure by formulating a "black box" optimization problem. Section IV provides empirical results. Section V provides a conclusion and future work.

II. Power System and Controls Model

A. Power System Dynamic Model

To explore the qualitative features of the proposed adaptive power flow-based generator controls, this work utilizes the small test power system model shown schematically in Fig. 1. The model is an expansion of the IEEE 9-bus test case [7] where one additional generator is connected to bus 8 via two additional transmission lines. The transient synchronous generator models in Fig. 1 are four fourth-order and use lead-lag transfer functions to model the d and q-axis inductances [6]. Generator voltage dynamics are described by a third-order exciter model that is controlled using an Automatic Voltage Regulator (AVR) which includes simple proportional control on the generator's terminal voltage magnitude. The loads are constant impedance. The details of the dynamic model used are found in [6].

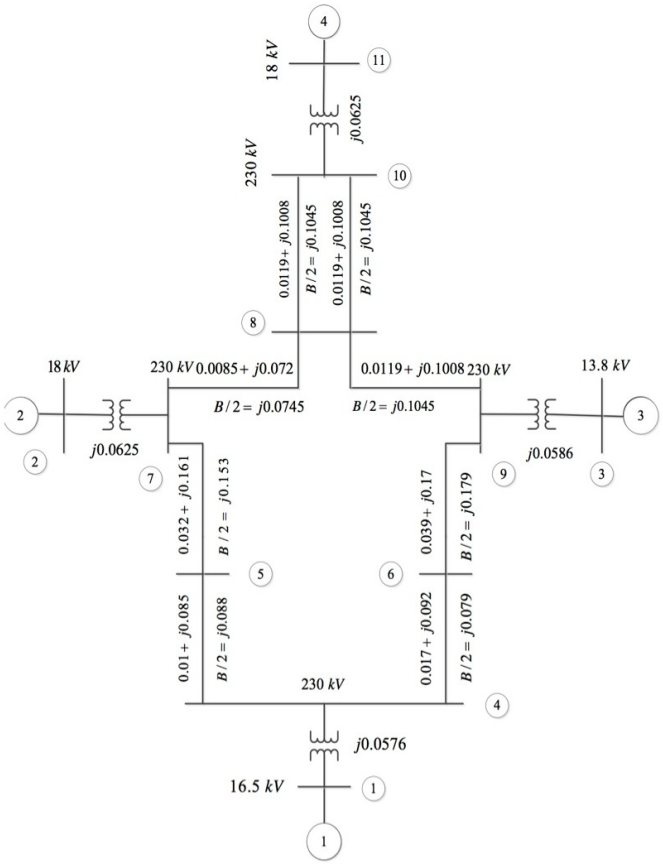

Fig. 1: A one-line diagram of the test case used in this work. The test case is an expansion of the IEEE-9 bus test case and includes four synchronous generators that are described using fourth-order generator models, third-order exciter models, first-order turbine governor models and constant impedance loads. Standard AVR is used to control generator terminal voltage, however, the generator governors are modified to include the power flow inputs described in Sec. II-B in addition to the usual speed droop.

B. Turbine Governor Dynamics With Power Flow Inputs

Our new control measures the deviation in real power flows on lines adjacent to each generator and modifies the normal speed droop control signal by adding inputs to the generators' governors. Incorporation of this control in the system model modifies the governor state variables and requires some care. Here, we provide some details of the implementation.

Figure 2 shows a block diagram of the IEEE Type 2 turbine governor used in this work. The dynamics of this governor are

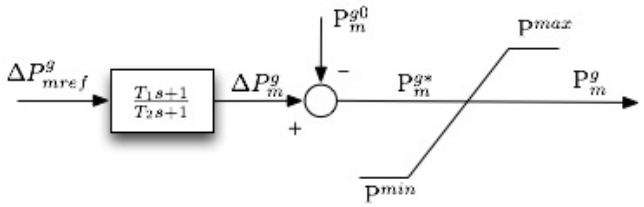

Fig. 2: The block diagram structure of the standard IEEE Type 2 turbine governor used in this paper. Our modification to the governor is though the input ΔP^g_{mref} described in Eq. 4.

described by

$$\dot{x}_{tg} = \frac{-1}{T_2}(x_{tg} + (1 - T_1/T_2)\Delta P^g_{mref}), \tag{1}$$

where x_{tg} is the state of the turbine governor, T_1 is the transient gain time constant, T_2 is the governor time constant, and ΔP^g_{mref} is the input to the governor. The output saturation relates the mechanical power input P^g_m to each generator to the dynamical variable P^{g*}_m by

$$P^g_m = \min(P^{max}, \max(P^{min}, P^{g*}_m)). \tag{2}$$

Here, P^{g*}_m is related to the governor's state variable x_{tg} by

$$P^{g*}_m = x_{tg} - \frac{T_1}{T_2}\Delta P^g_{mref} + P^{g0}_m. \tag{3}$$

Normally, ΔP^g_{mref} is only the speed droop signal. Our new control incorporates signals from real power flow deviations on lines adjacent to each generator i, i.e.

$$\Delta P^i_{mref} = \gamma_i(\omega_i(t) - \omega_0) + \sum_{j \in \mathcal{L}_i} \lambda^j_i (P_j(t) - P_j(0)). \tag{4}$$

The first term on the right hand side (RHS) is the normal speed droop input where $\omega_i(t)$ is the frequency at generator i at time t, ω_0 is the nominal system frequency, and γ_i is the speed droop gain. Throughout this manuscript, we will take γ_i =0.04. The second term on the RHS is the power flow-based control where $P_j(t)$ is the real power flowing on line j at time t, $P_j(0)$ is the nominal steady-state power flow on line j, $\mathcal{L}_i$ is the set of lines adjacent to generator i, and λ^j_i are power flow control gains. We will denote the set of power flow gains at a single generator as λ_i and the entire set of power flow gains as λ. The set of gains λ are chosen through the optimization method described in Sec. III-C.

C. Simulation Details

The power system dynamics are simulated using the Power System Analysis Toolbox (PSAT) [6]. The initialization of the state variables is modified to include the new controls described above, and the integration is carried out using the trapezoidal method. After a short simulation period to ensure the system is in steady state, a contingency is applied. The set of contingencies $C_i = (b_i, t_{0,i})$ is defined as three phase faults at bus b_i of duration $t_{0,i}$. The fault-on period lasts for time $t_{0,i}$ after which the fault is cleared and the time simulation continues. The duration of the simulation depends on the definition of the stability metric discussed in Sec. III-A

III. Adaptive Control Optimization

The goal of introducing the power flow-based control in Sec. II-B is to improve the transient stability of the post-contingency dynamics. We propose to use optimization to set the power flow deviation gains and to make this control adaptive to changing system conditions. Below, we discuss a penalty function that approximates the proximity to instability for each contingency C_i, the aggregation of individual penalties into a system penalty, and the optimization used to reduce the system penalty below an empirically determined threshold.

A. Contingency-Specific Penalty

The dynamical simulations described above are used to compute a metric that measures the proximity of the post-fault dynamics to instability. The metric is computed for contingency C_i, initial system state x^0 and the power flow control parameters λ. All other parameters are assumed to be fixed. The metric M utilizes two key stability measures and is defined as:

$$M(C_i, x^0, \lambda) = \frac{1}{T}\int_{t_f}^{t_f+T} \left[\alpha \sum_{i \in G}\left(\frac{\omega_i(t) - \bar{\omega}(t)}{\omega_0}\right)^2 + \sum_{i \in N}\left(\frac{V_i(t) - V_i(0)}{V_i(0)}\right)^2\right] a(t)dt \tag{5}$$

The first term penalizes the dispersion of the frequencies at the generators (i.e. at buses G) from the system average frequency $\bar{\omega}(t)$. The dispersion is defined relative to the average frequency rather than ω_0 to limit the interaction between the new power flow-based control and the normal behavior of speed droop control. The second term penalizes the dispersion of the voltage magnitudes $V_i(t)$ (at all system buses N) from their prefault values $V_i(0)$.

The integral of these two terms is calculated over a specified time horizon beginning at the moment the fault is cleared, t_f and ending at $t_f + T$. In this work, we find that T = 5 seconds is sufficient for the purpose of approximating the penalty function for optimization. α is an adjustable weight between the frequency and voltage dispersion penalties. The weighting function $a(t) = 1 - e^{-t/\tau}$ emphasizes times later in the post-contingency time horizon. In this work, we find $\alpha = 1000$ and $\tau = 5$ seconds give satisfactory results, although no systematic study of these parameters was performed.

Figure 3 displays the behavior of the stability metric and its components for faults on bus 4 of different duration where the only controls were the usual speed droop and AVR, i.e. no additional power flow controls. For short fault durations, both the frequency and voltage components (and the total stability metric) are quite small. As the duration increases, the penalty components and the total increase monotonically. Figures 4 and 5 display the results of simulations that were used to

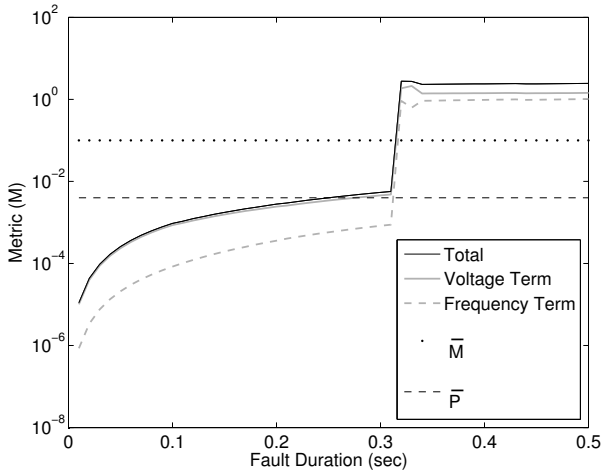

Fig. 3: Stability metric M versus fault duration for a fault at bus 4 in Fig. 1. As the duration of the fault increases, M increases smoothly and monotonically until a fault duration of $\sim$0.31 seconds where the post-fault dynamics display loss of generator synchrony. Prior to this critical clearing time, M provides a reliable measure of the proximity to instability. Beyond this critical clearing time, the simulation results in an erratic and non-monotonic M that cannot be used for the optimization of the power flow gains λ.

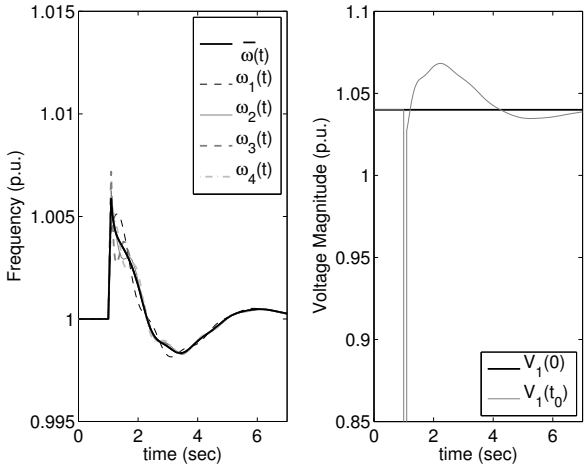

Fig. 4: Simulated transient response for a fault at bus 4 of duration 0.10 seconds used to compute the stability metric M in Fig. 3. The left plot shows the frequency ω_i at each of the four generators and the system average frequency. The right hand plot shows the voltage at bus 1 and its value prior to the fault.

compute the stability metric in Fig. 3 for fault durations 0.10 seconds and 0.3 seconds, respectively. The fault is applied at t_0 = 1 second. The results for the longer fault duration in Fig. 5 show much larger differences in individual generator frequencies which implies larger dynamical phase differences and dynamics that are closer to loss of synchrony. This is also reflected in the stability metric which is 0.0021 and 0.0106 in Figs 4 and 5, respectively.

The stability metric M is well behaved until a duration of approximately 0.31 seconds where the simulation shows the post-fault dynamics result in loss of generator synchrony. Below the transition, the metric M provides a measure of the proximity to instability. Above the transition, the simulation results yield a metric M that is no longer monotonic and is no longer a reliable measure of the proximity to instability. To avoid numerical issues associated with the behavior of M beyond the critical clearing time, an upper bound $\bar{M}$ is placed on M. The resulting contingency-specific penalty $P(C_i, x^0, \lambda)$ is given by

$$P(C_i, x^0, \lambda) = \min(M(C_i, x^0, \lambda), \bar{M}). \quad (6)$$

For the rest of the paper we will abuse notation by writing $P(C_i, x^0, \lambda)$ as P_i and $M(C_i, x^0, \lambda)$ as M_i when context is clear.

Using the results in Fig. 3 and similar results for other contingencies as guidance, we set $\bar{M}$=0.1 for the remainder of this manuscript (also shown in Fig 3). However, we note that the optimization procedure described below will seek to avoid situations where Eq. 6 forces $P = \bar{M}$.

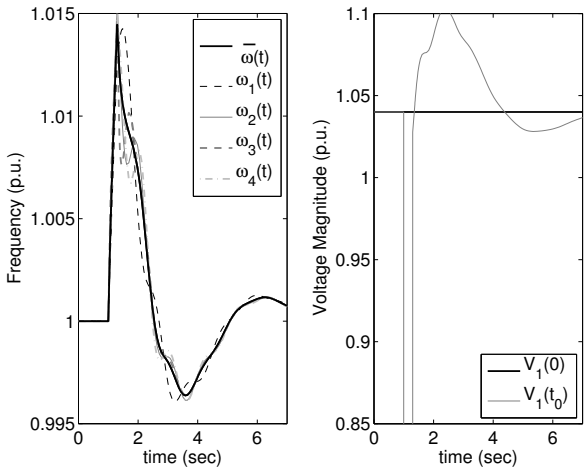

Fig. 5: Same as Fig. 4 but for a fault duration of 0.3 seconds.

B. System-Wide Penalty

The goal of our new power flow controls is to create stable dynamics for the entire set of contingencies C. Therefore, the contingency-specific penalty defined above should be aggregated into a system-wide penalty. In addition, the control should maintain a quantifiable stability margin. To these ends, we suggest the following system-wide penalty:

$$P_{sys} = \Sigma_{i \in C} \max(0, P_i - \bar{P}_i) \quad (7)$$

where $\bar{P}_i$ is a threshold value for contingency i that is set below the value of P_i where the system loses stability. Currently, we determine this value empirically. A threshold value of 0.004 is chosen for a fault on bus 4 and is shown in Fig. 3. The threshold for all faults range from 0.004 to 0.0114. Using a threshold to maintain a stability margin has additional benefits discussed below.

C. Adaptive Optimization

Using the penalty P_{sys} from Eq. 7, we perform an optimization over the set of gains λ for each generator governor in the system. The optimization is solved using an interior point gradient descent method that computes numerical gradients [8] using the PSAT dynamical simulations as a "black box" evaluator. Each iteration of the gradient descent requires several evaluations of P_{sys}, i.e. several dynamical simulations to evaluate the individual P_i. However, the structure of P_{sys} provides several advantages.

Including non-zero thresholds $\bar{P}_i$ in P_{sys} allows the optimization to terminate when it finds an set of control gains with an acceptable stability margin without excessively iterating to find a local minimum in the P_i. Additionally, by maintaining a stability margin, each of the P_i is kept sufficiently far from the transition to instability that the gradient in P_{sys} is well behaved. However, depending on how the algorithm is initialized, a contingency k may have $P_k = \bar{M}_k$. In this case, we temporarily decrease the fault duration time $t_{0,k}$ until $P_k < \bar{M}_k$ and run the optimization until $P_{sys} = 0$. At this point, $P_k = \bar{P}_k$. The fault duration $t_{0,k}$ is increased and the process repeated until $t_{0,k}$ reaches its original value with $P_k < \bar{M}_k$ at which point the optimization procedure can be executed normally.

The structure of P_{sys} suggests another numerical simplification which is not fully exploited in this manuscript but will be leveraged in future work on larger power system models. If a contingency C_i has $P_i < \bar{P}_i$, then it makes no contribution to the overall system penalty P_{sys} and does not need to be evaluated by time consuming dynamical simulation during the optimization. This observation suggests a cutting plane-like approach where, after an initial evaluation to determine the P_i, only the C_i with $P_i > \bar{P}_i$ are retained in the optimization procedure. Once the procedure finds a set λ such that $P_{sys} = 0$, a screening of all the C_i is again performed to check if the control has caused any of the previously ignored C_i to now also have $P_i > \bar{P}_i$. If additional C_i are found, they are included in the set that contributes to P_{sys} and the optimization procedure is repeated until no new C_i are found.

Power system conditions will evolve over the operating day because of the nominally repeatable changes in the magnitude and configuration of load and because of the less repeatable changes in intermittent generation such as wind and photovoltaic generation. As the system changes, the set of contingencies that result in unstable dynamics will also evolve. We envision that the optimization procedure described above would be executed periodically in an off-line fashion to compute an updated set of feedback parameters that would be distributed to the generators on the time scale of economic dispatch signals.

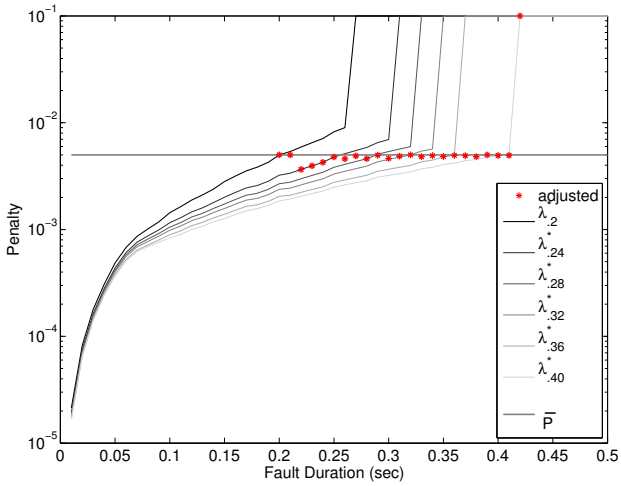

Fig. 6: Penalty for a fault at bus 8 versus the fault duration different values of the gains λ. Starting with a fault duration of 0.2, we the optimize the gains λ until the penalty is below the threshold $\bar{P}$ (horizontal line). Using these new gains, the penalty versus fault duration curve is computed again (the $\lambda_{.24}$ curve) showing that $\bar{P}$ is exceeded at a fault duration of 0.24 seconds. This process is repeated multiple times resulting in series of curves in the Figure.

IV. Empirical Results

A. Preliminary Results–Single Fault

When considering the entire set of contingencies C, the behavior of the power system and the optimization can be quite complex. To demonstrate our approach and to build some intuition about the results, we consider a simplified case where we study a single fault on bus 8 in Fig. 1. Starting with $\lambda = 0$, i.e. considering only speed droop and AVR, we scan over a range of fault durations and map out the upper left curve in Fig. 6. Much like Fig. 3, the penalty value P_8 grows as the fault duration increases until it exceeds the threshold ($\bar{P}_8$ =0.005) at a duration of approximately 0.20 seconds. We continue the penalty calculation beyond this duration for illustration purposes only.

At a duration of 0.20 seconds and considering only the fault on bus 8, we execute the optimization procedure looking for a set of gains λ that result in $P_8 = \bar{P}_8$ =0.005. The finite step of the optimization actually results in $P_8 < \bar{P}_8$. For illustration purposes, we use the computed gains λ and once again scan over a range of fault durations for bus 8 finding that $P_8 > \bar{P}_8$ for a fault duration of 0.24 seconds (see the $\lambda_{.24}$ curve in Fig. 6). The optimization process is repeated to generate an updated set of gains λ. Another scan over fault duration shows these gains result in $P_8 > \bar{P}_8$ at a duration of 0.28 seconds (see the $\lambda_{.28}$ curve). This process is repeated until a set of gains λ are found that result in $P_8 < \bar{P}_8$ out to a fault duration of 0.40 seconds. Beyond this duration, the optimization fails to find a feasible solution.

The example in Fig. 6 demonstrates the initialization procedures described in Sec. III-C. By starting with a fault duration time of 0.20 seconds, we are able to incrementally find sets of gains λ that enable longer fault durations before the dynamics become unstable. Starting from λ =0 in Fig. 6, it took three iterations until the optimization could find a feasible solution for a fault duration of 0.30 seconds. The results in Fig. 6 suggest another advantageous property of the control method and optimization procedure we have proposed. The curves generated by optimizing for a fault duration t_0 fall entirely below the penalty for a curves generated by optimizing for any fault duration less than t_0. If this observation were to hold for all faults, optimizing for a fault duration of say 0.30 seconds would always result in improved performance for shorter fault durations.

B. Main Results–Uniform Load Growth

Next, we perform a system study that considers faults at buses 4-9. In this case, we restrict the study to a uniform fault clearing time applied to these buses, i.e. we would like the post-fault dynamics for each bus to maintain a margin of stability for a fault clearing time of 0.24 seconds. Instead of varying the fault clearing time, we vary the load on the system by uniformly scaling the load at all buses while also uniformly increasing the injections at all generator buses. Any difference in the system losses is taken up by the generator at the slack bus, bus 1. This study emulates the evolution of a power system through a day with load starting at relatively low levels and slowly increasing toward its daily peak.

For the 11-bus test system in Fig. 1, we consider faults at buses 4 through 9. In the rest of this discussion, we do not show results for faults on buses 4-6 because the post-fault dynamics for these buses are stable under all conditions considered in this study. Figure 7a displays the penalties P_7, P_8, and P_9 for load/generation scaling factors ranging from 0.5 to 1.35 when the generator controls are only speed droop and AVR. These three faults result in unstable post-fault dynamics for load scaling in the range 1.1-1.2 and with associated penalties slightly above 0.010. To maintain a reasonable stability margin, the penalty thresholds are set below the penalties where the transitions occur, i.e. $\bar{P}_7 = 0.0114$, $\bar{P}_8 = 0.0107$, $\bar{P}_9 = 0.0091$.

A close up view of the results for the faults on buses 7, 8, and 9 are shown in Figs. 7 b), c), and d), respectively. The curves labeled λ^0 in these Figures repeat the results from Fig. 7a showing the penalties in relation to the penalty thresholds (horizontal lines) for the individual buses as a function of the load scaling for generators controlled only by speed droop and AVR. Starting at a low load scaling (less than 0.9), all buses show acceptable post-fault dynamics on the λ^0 curve, i.e. the stability margins are respected when only speed droop and AVR are used. As the load increases along the λ^0 curve to a load scaling of 1.0, the faults on buses 7 and 8 show penalties that exceed their thresholds. At this system condition, we carry out our optimization procedure and find a set of gains λ^1 that reduce P_7 and P_8 below their thresholds. Although P_9 had not exceeded its threshold and did not factor directly into the optimization, the gains λ^1 also reduce P_9.

Load on the power system continues to increase, but now the system traverses the λ^1 curves. At a load scaling of 1.1, P_7 and P_8 once again hit their thresholds. Our optimization is run once again resulting in gains λ^2 that push P_7 and P_8 below their thresholds. P_9 is once again reduced. The power system now traverses the λ^2 curve. Further increases in power result in two more repetitions of this process finally resulting in gains λ^4. At this point, the use of feedback on power flow deviations has allowed the load on the power system to be increased by 20% over the load that would have originally caused encroachment on the dynamical stability margins.

Finally, Figure 8b visualizes the behavior of the power flow terms. Interestingly, in this case, the magnitude of the control parameters monotonically change as the load increases. This is a nice feature of the control and future work will investigate the prevalence and potential theoretical justification for this behavior.

V. Conclusion and Future Work

Standard generator controls consisting of speed droop and automatic voltage regulation (AVR) contribute to the stability of power system dynamics following a contingency such as a normally cleared fault. When a power system is stressed, this set of controls may be insufficient to maintain transient stability. We introduced a modification to these controls that includes additional inputs to a generator's governor derived from measurements of the deviations of power flows on lines adjacent to the generator from their nominal steady state values. We introduced an optimization procedure that discovers gains for these new governor inputs that reduce the post-fault dispersion of generator frequency relative to the system average frequency and the dispersion of the nodal voltages from their pre-fault values. Using a small test model, we find that this optimization procedure enhances the region of transient stability, allowing the test system to be loaded beyond a level that would result in unstable post-fault dynamics if the only speed droop and AVR were employed.

There remain a number of interesting future directions for this work. The power system model used in this work was quite small and a fault applied at any bus in the model directly affected every generator in the system. Larger models will enable the exploration of localization of generator response to specific faults. Larger systems will also test the ability of this method to handle larger dynamical systems and exercise optimization approaches such as cutting plane techniques to handle a larger number of fault scenarios without severely impacting the computational tractibility. We also plan to explore fast stability screening methods, like Lyapunov functions, to identify the initial set of unstable contingencies. Finally, additional classes of contingencies should be included beyond normally-cleared faults.

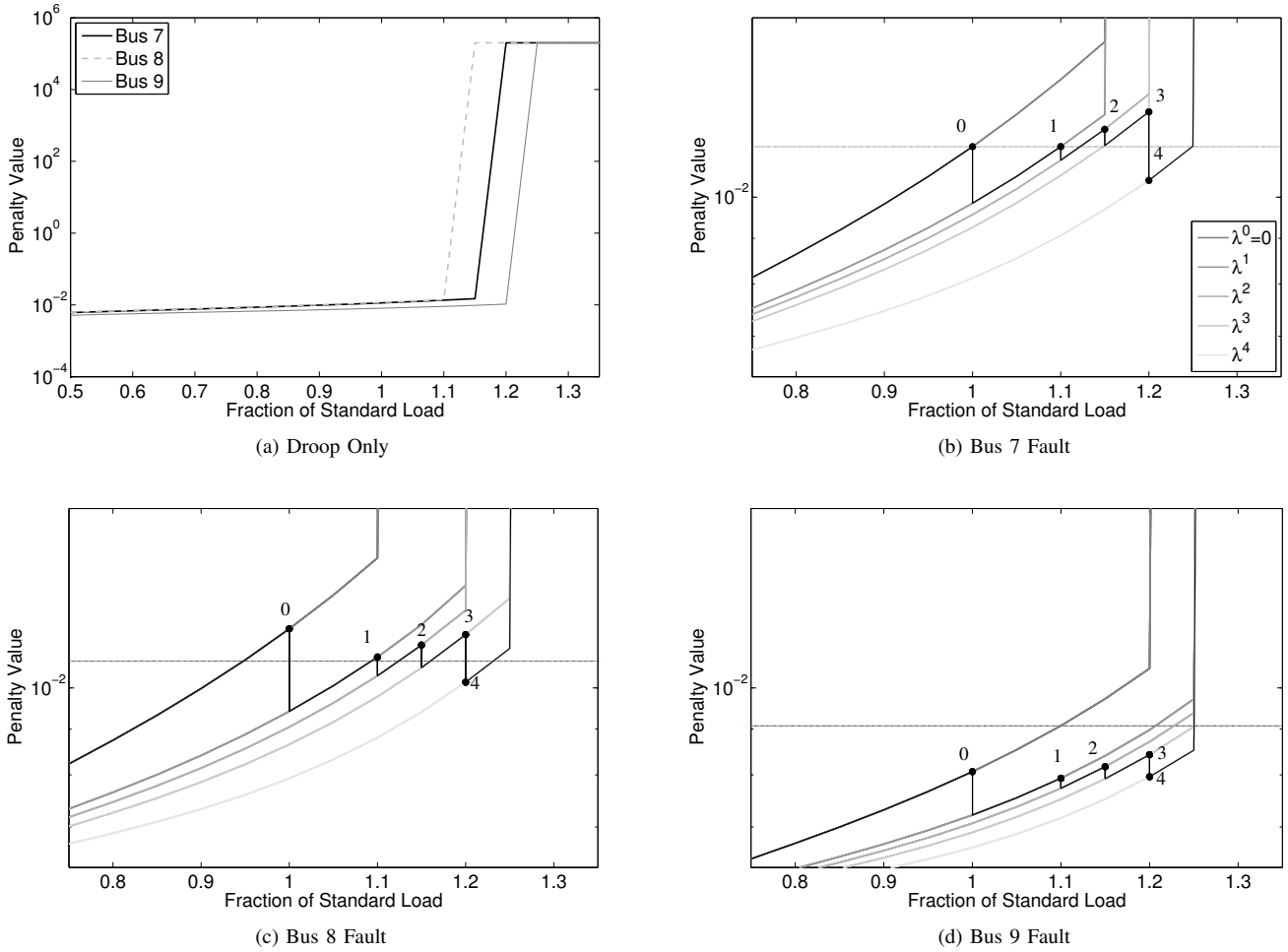

(a) Droop Only

(b) Bus 7 Fault

(c) Bus 8 Fault

(d) Bus 9 Fault

Fig. 7: Progression of the penalties for faults on buses 7, 8, and 9 as a function of the scaling of the system load in Fig. 1. a) Variation of the penalties P_7, P_8, and P_9 for generators controlled only by speed droop and AVR. b) Variation of the penalty P_7 for different sets of power flow deviation gains λ found using the optimization procedure described in Sec. III-C. The numbered curves index different runs of the optimization algorithm. The horizontal line is the penalty threshold $\bar{P}_7$. b) Same as a) except for bus 8. c) Same as a) except for bus 9.

Generator	Line 1	Line 2
1	4-5	4-6
2	7-5	7-8
3	9-6	9-8
4	10-8	10-8

(a) Generator-Parameter Mapping

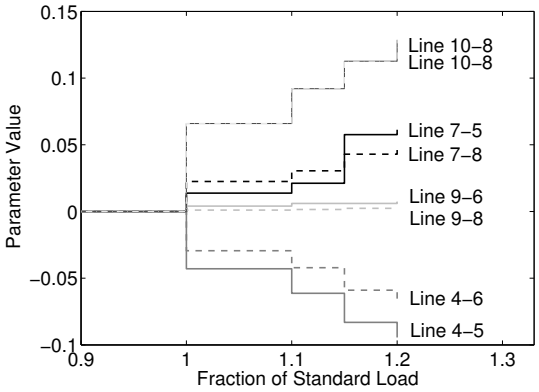

(b) Parameter Evolution

Fig. 8: a) A table mapping each generator in the system to their corresponding power flow measurements. b) The evolution of the power flow deviation gains λ versus the load scaling. Parameters monotonically change as the load increases.

REFERENCES

[1] J Liang R G Harley D Molina, G K Venaygamoorthy. Intelligent local area signals based damping of power system oscillations using virtual generators and approximate dynamic programming. *IEEE Trans. on Smart Grid*, 4(1), 2013.

[2] M Chertkov F Bullo F Dörfler, M R Jovanović. Sparse and optimal wide-area damping control in power networks. In *American Control Conference*, 2013.

[3] Y Hébert I Kamwa, R Grondin. Wide-area measurement based stabilizing control of large power systems - a decentralized/hierarchial approach. *IEEE Transactions on Power Systems*, 16(1), February 2001.

[4] S Bauckhaus K Dvijotham and M Chertkov. Distributed control of generation in a transmission grid with a high penetration of renewables. In *IEEE SmartGrid Comm: Symp. on Architectures and Models for the Smart Grid*, 2012.

[5] Kundur. *Power System Stability and Control*. McGraw-Hill, 1994.

[6] F Milano. *Power System Analysis Toolbox*, 2.1.6 edition, 2010.

[7] IEEE Committee Report. Current usage and suggested practices in power system stability simulations for synchronous machines. *IEEE Trans. Energy Conversion*, 1:77–93, 1986.

[8] MATLAB Optimization Toolbox. *version8.3 (R2014a)*. The MathWorks Inc., 2014.

[9] Yi Zhang and Kevin Tomsovic. Adaptive remedial action scheme based on transient energy analysis. In *Power Systems Conference and Exposition*, 2004.